nature chemistry

ARTICLES

PUBLISHED ONLINE: 25 MARCH 2012 | DOI: 10.1038/NCHEM.1303

Elucidation of the timescales and origins of quantum electronic coherence in LHCII

Gabriela S. Schlau-Cohen[1,2†], Akihito Ishizaki[1,2†], Tessa R. Calhoun[1,2†], Naomi S. Ginsberg[1,2], Matteo Ballottari[3], Roberto Bassi[3] and Graham R. Fleming[1,2*]

Photosynthetic organisms harvest sunlight with near unity quantum efficiency. The complexity of the electronic structure and energy transfer pathways within networks of photosynthetic pigment–protein complexes often obscures the mechanisms behind the efficient light-absorption-to-charge conversion process. Recent experiments, particularly using two-dimensional spectroscopy, have detected long-lived quantum coherence, which theory suggests may contribute to the effectiveness of photosynthetic energy transfer. Here, we present a new, direct method to access coherence signals: a coherence-specific polarization sequence, which isolates the excitonic coherence features from the population signals that usually dominate two-dimensional spectra. With this polarization sequence, we elucidate coherent dynamics and determine the overall measurable lifetime of excitonic coherence in the major light-harvesting complex of photosystem II. Coherence decays on two distinct timescales of 47 fs and ~800 fs. We present theoretical calculations to show that these two timescales are from weakly and moderately strongly coupled pigments, respectively.

Photosynthetic organisms fuel most life on Earth by absorbing sunlight and converting it to chemical energy with near unity quantum efficiency[1]. Networks of densely packed pigment–protein complexes (PPCs) absorb and then translocate photoenergy to a central site of charge separation, known as the reaction centre[2]. The relatively low intensity of sunlight at the Earth's surface (1,000 W m^{-2}) drives the dense packing of pigments within PPCs, which produces electrodynamic couplings between pigments. These couplings are highly sensitive to molecular structure, and their strength determines the pathways and mechanisms by which energy is transported from an initial absorption site to the reaction centre[3]. Furthermore, strong couplings enable the existence of quantum-coherent electronic excitations between multiple pigments, even at physiological temperatures[4,5]. We describe a new extension of two-dimensional (2D) spectroscopy, the application of a coherence-specific polarization sequence, which directly probes quantum coherence. This technique explores and isolates coherence-related phenomena, including those that arise from coherence transfer.

Emerging experimental and theoretical results have revealed that electronic excitations move through photosynthetic complexes as quantum-mechanical wave packets that maintain their phase coherence[6,7] or exhibit long-lasting oscillatory motion between multiple pigments. This effect, quantum coherence, involves a coherent superposition of delocalized excited states, which theoretical results have suggested could be one potential contributor to the remarkable efficacy of photosynthetic light harvesting[8–11]. Long-standing experiments have observed indications of quantum coherence, but only recently have 2D and non-degenerate photon echo experiments begun to provide methods to clearly access signals from quantum coherence[4,6,12–14]. These four-wave-mixing experiments have detected long-lived quantum coherence in PPCs from bacterial, algal and plant systems at ambient and cryogenic temperatures[4,5,13,15]. Although the existence of coherence has been observed at both physiological and cryogenic temperatures, questions remain about the functional significance of coherence and its contribution to light harvesting.

Existing techniques are able to detect signals from coherence persisting over durations much longer than the femtosecond timescale of typical energy transfer steps in photosynthesis[5]. The coincidence of timescales stimulates discussions on whether coherence may play a role in ensuring the efficiency of energy transfer. One component of understanding the role of quantum coherence in excitation energy transfer is quantifying the relationship between long-lived quantum beating and donor/acceptor states. This requires elucidating the energies of excitonic states exhibiting strong quantum beating and comparing them to energies of donor and acceptor states, and then finding timescales over which quantum beating signals decay and comparing them to the timescales of energy transfer. Correlating the lifetime of beating and the rate of energy transfer may allow for a better understanding of the interplay between them.

In this Article, we demonstrate a new method for studying electronic coherence through the application of the coherence-specific pulse polarization sequence (45°, −45°, 90°, 0°)[16]. The resultant 2D spectra map the evolution of excited-state coherences free from a background of traditional diagonal signals and energy transfer peaks[16–18]. Without collecting a large number of timepoints to sample the oscillations, individual spectra can show both the lifetimes of excited-state coherences and their excitation and emission energies.

In 2D spectroscopy, a broadband femtosecond pulse, encompassing multiple transitions, excites the sample and then monitors its evolution by spectrally resolving both absorption and emission frequencies as a function of a variable temporal delay (the time period over which quantum coherence is observed) between

[1]Department of Chemistry, University of California, Berkeley, California 94720, USA, [2]Physical Biosciences Division, Lawrence Berkeley National Laboratory, Berkeley, California 94720, USA, [3]Dipartimento di Biotecnologie, Facoltà di Scienze, Università di Verona, Strada Le Grazie, I-37134 Verona, Italia, [†]Present address: Department of Chemistry, Stanford University, Stanford, California 94305, USA (G.S.S-C.), Institute for Molecular Science, National Institutes of Natural Sciences, Okazaki 444-8585, Japan (A.I.), Lewis-Sigler Institue for Integrative Genomics, Princeton University, Princeton, New Jersey 08544, USA (T.R.C.). *e-mail: grfleming@lbl.gov

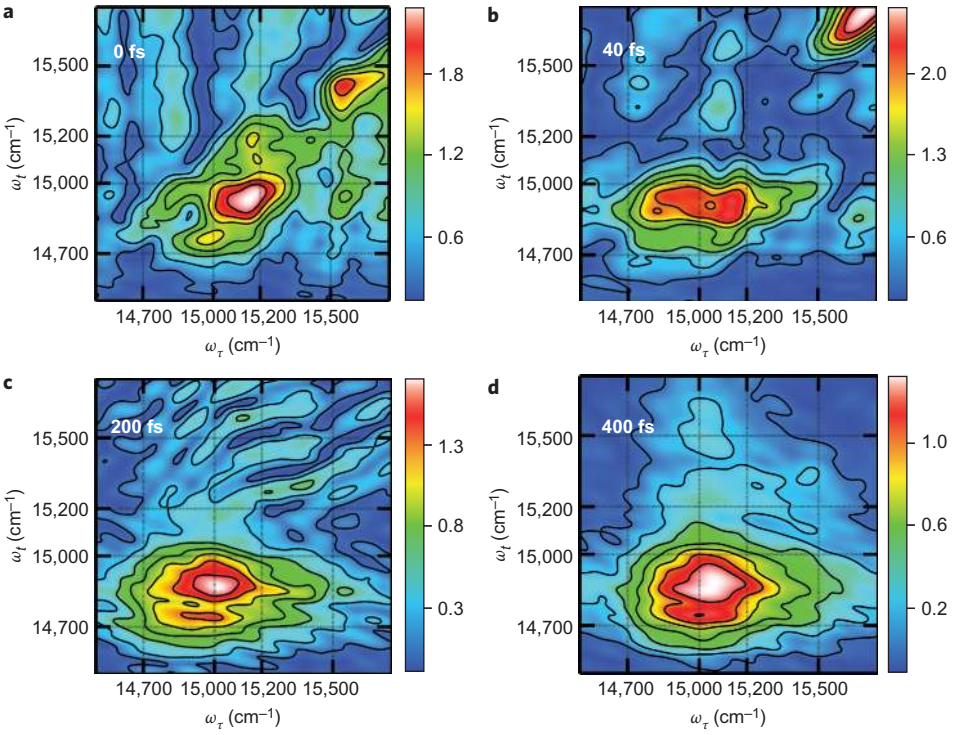

Figure 1 | Absolute-value non-rephasing spectra under coherence-specific polarization at 77 K. a, $T = 0$ fs. **b**, $T = 40$ fs. **c**, $T = 200$ fs. **d**, $T = 400$ fs. Owing to the polarization of the incident pulses, these spectra contain only peaks corresponding to quantum coherences. The appearance of peaks along the diagonal in **a** shows the existence of quantum coherence in all spectral regions. The relatively high intensity of the mid-energy Chl-*a* peak (~14,900 cm^{-1}) indicates a stronger coherence contribution within this region than seen previously and than was predicted by previous models.

absorption and emission events[19–22]. The 2D spectra are plotted as a function of absorption (ω_τ) and emission (ω_t) frequency for each delay time (T) and contain the sum of all phase and energy-conserving processes within the system, including absorption, energy transfer, coupling and coherence[19,20]. A 2D measurement requires interaction with four laser pulses. Careful manipulation of their polarization reveals information about molecular processes normally obscured by more intense, overlapping peaks[23–25]. By varying the polarization of the incident pulses, we generate coherence-specific spectra to examine the energies and timescales of excited states that give rise to quantum coherence. The spectra are free from a background of signals corresponding to absorption and emission processes, population transfer, electronic coupling and excited-state absorption. The two excitation pulses are orthogonal to one another, as are the two emission pulses. This selects for Liouville pathways where, in the ensemble, the two pulses can only both interact with transition dipoles that have a component perpendicular to each other, or are non-parallel[26]. In the case of exciting a population, $\rho = |e_1\rangle\langle e_1|$, the two transition dipoles are of the same state, and thus are necessarily parallel to each other (themselves). Thus, for orthogonal excitation pulses, the system is excited into a coherence, $\rho = |e_1\rangle\langle e_2|$. Pulse 3 and the detected (local oscillator) polarization are also orthogonal, and so only detect signals emitted from a coherence. The ability to observe the isolated coherence signal allows a clearer understanding of which excited states contribute to coherent motion and therefore how excitonic coherence coincides with, and so contributes to, energy transfer.

In understanding photosynthetic light harvesting, studying light-harvesting complex II (LHCII) from green plants is critical because it contains more than 50% of the world's chlorophyll[27]. In recent all-parallel polarization 2D experiments on LHCII, the existence of coherence was demonstrated and observed to persist through the 500 fs timescale of the experiment at 77 K (ref. 15), which is notable because multiple energy transfer processes shorter than 500 fs have been observed within LHCII[24,28]. Although all-parallel 2D experiments determined the existence of long-lived quantum beating signals[6,15], the long data collection times required to resolve multiple oscillation periods of quantum beats precluded examination of quantum coherence through the decay of the oscillation. Additionally, determining decay times by sampling oscillatory behaviour requires fitting the frequency and decay of each quantum beating component. In congested systems, such as photosynthetic PPCs, closely spaced, overlapping transitions mean beating signals contain multiple frequency components. Analysis of oscillations with multiple frequency components is easily contaminated by laser fluctuations and other sources of experimental noise, as these also give rise to alternately increasing and decreasing intensities. Here, we apply the coherence-specific polarization scheme to LHCII. Under coherence-specific polarization, peaks arise only at the energies of excited states exhibiting coherences. Thus, these spectra provide new information about which individual excited states exhibit quantum coherence, the lifetime of coherence within each spectral region and the overall measurable lifetime of this phenomenon in LHCII. This allows for examination over a larger range of delay times, useful for analyses such as determining the lifetime of coherence.

Results

Trimeric LHCII comprises three monomers, each with 14 chlorophyll and four carotenoids, with the pigments in a close-packed arrangement inside a surrounding protein matrix[29,30]. The 14 chlorophylls are found in two spectral and structural variants (eight Chl-*a* and six Chl-*b*). In Fig. 1a–d, absolute-value, non-rephasing 2D spectra under the coherence-specific polarization sequence are shown. Tickmarks divide the spectra into three regions: (i) Chl-*a* (14,700–15,000 cm^{-1}); (ii) intermediate, with high-energy Chl-*a* and low-energy Chl-*b* (15,000–15,200 cm^{-1}); (iii) Chl-*b* (>15,200 cm^{-1}). The spectra are characterized by three diagonal

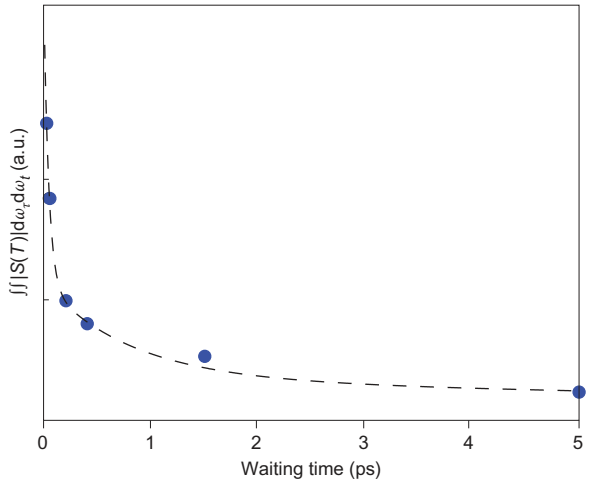

Figure 2 | Integrated, absolute-value relaxation spectra taken under coherence-specific polarization plotted versus waiting time. Fitting of this curve (Table 1) allows for extraction of the timescales of the dephasing of quantum coherence in LHCII. The steep decay at early times most likely arises from short-lived coherences between excited states on weakly coupled chromophores, while the intermediate decay time (700–900 fs) shows the dephasing of coherences between excited states on strongly coupled chromophores. The 700–900 fs timescale of coherences is longer than many energy transfer steps within LHCII.

peaks: two peaks in the Chl-*a* region (low- and mid-energy Chl-*a*) and one peak in the Chl-*b* region. The signals due to coherence give rise to on-diagonal and off-diagonal contributions, which appear in non-rephasing and rephasing spectra, respectively[31]. The time-ordering of pulses 1 and 2 differentiates the non-rephasing (pulse 2, pulse 1) and rephasing (pulse 1, pulse 2) spectra[32]. The coordinates of off-diagonal peaks, which appear in the rephasing spectra, connect the two excitons that give rise to the superposition state. Within the non-rephasing spectra, diagonal features directly correspond to each exciton involved in quantum coherence and so provide a direct measure, weighted by the orientational factor and dipole strength of these transitions, of the amount of excitonic coherence in which each state is involved. Additionally, the antidiagonal elongation of the non-rephasing features facilitates the identification of excited-state energies[31].

In the Fig. 1 spectra, all Liouville pathways that do not arise from coherence during the waiting time are suppressed[16,17] due to the pulse polarizations (45°, −45°, 90°, 0°). Signal scaling with pulse polarization arises from an orientational prefactor (described in detail in the first section of the Supplementary Information and shown in Supplementary Fig. S1), which is a function of the angle between pulse polarizations and the angle between the excited-state transition dipole moments. Even with the limited precision of experimental pulse polarizations, the intensities of population contributions are suppressed by up to orders of magnitude. As an example, we compare the orientational prefactors for two Liouville pathways under (0°, 0°, 0°, 0°) and (47°, −45°, 90°, 0°): the orientational prefactor of $R_1^{(ii)}$ goes from 0.200 to 0.002 and the orientational prefactor of $R_1^{(ij)}$ goes from −0.07 to 0.082 for two excited states with $\theta_{ij} = 90°$, where *i*, *j* label exciton states. Thus, the population contributions have been suppressed by two orders of magnitude and the coherence contributions have been enhanced, even with a 2° error from ideal polarizations.

Diagonal features across the spectrum in Fig. 1a indicate the existence of coherence in all resonant regions. As observed in other 2D experiments on LHCII[15,24,28], diagonal signals appear shifted below the diagonal, even at $T = 0$ fs, and shift further with increasing waiting time. This is most probably due to relaxation along the potential energy surface during the pulse overlap interval, and the expected increase in the environmental relaxation with waiting time, showing essentially a time-dependent Stokes shift. Diagonal features in all resonant regions are consistent with the long-lived oscillatory behaviour observed in all-parallel 2D experiments on LHCII[15]. Here, however, the relative intensities of features in different spectral regions can be more easily observed because the population contributions have been removed. At $T > 0$ in particular, the mid-energy Chl-*a* region shows an especially intense peak, indicating that the Chl-*a* states that contribute to this feature exhibit strong, long-lived quantum beating. Thus, the mid-energy Chl-*a* states must contain states localized on chlorophyll strongly coupled to their neighbours. The chlorophyll that exhibit the strongest couplings within LHCII give rise to excited states in the mid-energy Chl-*a* region.

Coherence dephasing. Under coherence-specific polarization, the evolution of each peak displays the dynamics of each excited-state coherence, without the strong background of signals from populations. The large number of closely spaced, overlapping excited states, however, means that it is impossible to isolate the dynamics of each coherence. To gain insight into the general behaviour on the evolution of the coherences, we integrate the coherence-specific spectrum, $S(T, \omega_\tau, \omega_t)$, for each waiting time, and plot the integrated intensity versus waiting time (Fig. 2). This corresponds to

$$I(T) = \iint \left|S(T, \omega_\tau, \omega_t)\right| d\omega_\tau d\omega_t \approx \sum_{i,j} \left|S(T, \omega_i, \omega_j)\right| \Delta\omega_i \Delta\omega_j \quad (1)$$

Owing to the coherence-specific pulse sequence, we assume

$$S(T, \omega_i, \omega_j)\Delta\omega_i\Delta\omega_j \approx A_{ij} \cdot \rho_{ij}(T) \approx A_{ij}\, e^{\pm i(\omega_i - \omega_j)T} e^{-T/\tau_{ij}} \quad (2)$$

where $i \neq j$, $\{\rho_{ij}\}$ $\{\rho_{ij}(0) = 1\}$ are matrix elements of the density operator in the single-excitation manifold and $\{A_{ij}\}$ are constant values depending on oscillator strength, integration area, and so on. Thus, we obtain

$$I(T) \approx \sum_{i \neq j} A_{ij} \left|\rho_{ij}(T)\right| \approx \sum_{i \neq j} A_{ij}\, e^{-T/\tau_{ij}} \quad (3)$$

At short times, the time dependence of $I(T)$ is dominated by fast dephasing components (short-lived coherences), and the slow dephasing components (long-lived coherences) can be approximated as time-independent components,

$$\begin{aligned} I(T) &\approx \sum_{i \neq j} A_{ij} \left|\rho_{ij}^{\text{short-lived}}(T)\right| + \sum_{k \neq l} A_{kl} \left|\rho_{kl}^{\text{long-lived}}(T \approx 0)\right| \\ &\approx \sum_{i \neq j} A_{ij}\, e^{-T/\tau_{ij}^{\text{fast}}} + \sum_{k \neq l} A_{kl} \end{aligned} \quad (4)$$

At longer times, $I(T)$ can be approximated as

$$\begin{aligned} I(T) &\approx \sum_{i \neq j} A_{ij} \left|\rho_{ij}^{\text{short-lived}}(T \to \infty)\right| + \sum_{k \neq l} A_{kl} \left|\rho_{ij}^{\text{long-lived}}(T)\right| \\ &\approx 0 + \sum_{k \neq l} A_{kl}\, e^{-T/\tau_{kl}^{\text{slow}}} \end{aligned} \quad (5)$$

Because of a small contribution from suppressed signals due to experimental errors in polarization (~±2°), there is also a component, constant on the timescales of all coherences, of overall signal decay. Thus, the integrated intensity is fit to a three-lifetime exponential, and fit parameters are presented in Table 1. The short time and overall signal decay timescales (the shortest

Table 1 | Results of fitting the decay of the coherence-specific integrated spectral decay from Fig. 2.

Time constant (fs)	Amplitude (%)
46.5	64
809	24
13,740	11

The short time component arises from the coherences within weakly coupled chromophores. The intermediate component arises from the coherences within strongly coupled chromophores. The long time component arises from overall signal decay from processes such as annihilation.

and longest lifetime components) were determined through a bi-exponential fitting of integrated all-parallel data on LHCII taken on the same apparatus[28]. These two timescales represent the sum of the short-lived coherence decay, which dominates spectra under both polarizations at short times, and the overall signal decay. The overall signal decay is most probably primarily due to annihilation effects[33,34], which pump–probe experiments have observed induce decays on 16 and 24 ps timescales. Because in this power regime annihilation effects appear after energy transfer (if they occur via monomer–monomer transfer) and occur based solely on whether the system is in a ground state (no annihilation) or excited state (annihilation) during the waiting time, the decay time (although not the amplitude) should be independent of polarization sequence. The intermediate timescale, long-lived coherences, was found by fixing the short and long timescales in a tri-exponential fit of the coherence-specific data. This results in a decay time of the long-lived coherences of 700–900 fs at 77 K. The large range is due to (i) resolution from the limited number of data points and (ii) contributions from time evolution of the small amount of unsuppressed population transfer pathways, some of which increase and some of which decrease in amplitude with waiting time. Overall, however, the alternating increasing and decreasing intensities mostly cancel each other out by 1 ps, as shown by the evolution of the integrated intensity with waiting time under all-parallel polarization (Supplementary Fig. 2).

Theoretical results and discussion. A large number of coherences contribute to the integrated data presented in Fig. 2. Broadband femtosecond pulses initially excite coherent superpositions between many different combinations of the excitons in LHCII. A Fourier transform of oscillatory time-domain data from all-parallel 2D experiments[15] produced peaks at the energy differences between most of the excitonic states, but does not indicate the length of time they oscillate, because a single time-domain oscillation gives rise to a frequency-domain peak. To proceed with analysis of the present data, we consider two regions of electronic coupling strength. In the first category, the electronic coupling is on the same order or larger than the coupling to the surrounding protein environment. These coherences persist through the timescale of energy transfer, pointing to the existence of wavelike motion of the excitation through these pigments. In the second category, which contains most of these excitonic superpositions, these coherences simply arise because the excitation pulses encompass all Q_y transitions. The resultant oscillations decay rapidly because of vanishingly small couplings between these pigments. These oscillations carry no information about energy transfer dynamics. In Fig. 3, numerical calculations of the time evolution of quantum coherence between excitons are presented. The numerical calculations were performed with the second-order cumulant time-convolution quantum master equation[35], which describes excitation energy transfer dynamics accurately. The Hamiltonian values of ref. 24 were used with modifications from ref. 28, and all calculations were for 77 K. At present, no direct and detailed information is available regarding the pigment–protein interactions in LHCII at 77 K (that is, the bath spectral density). We

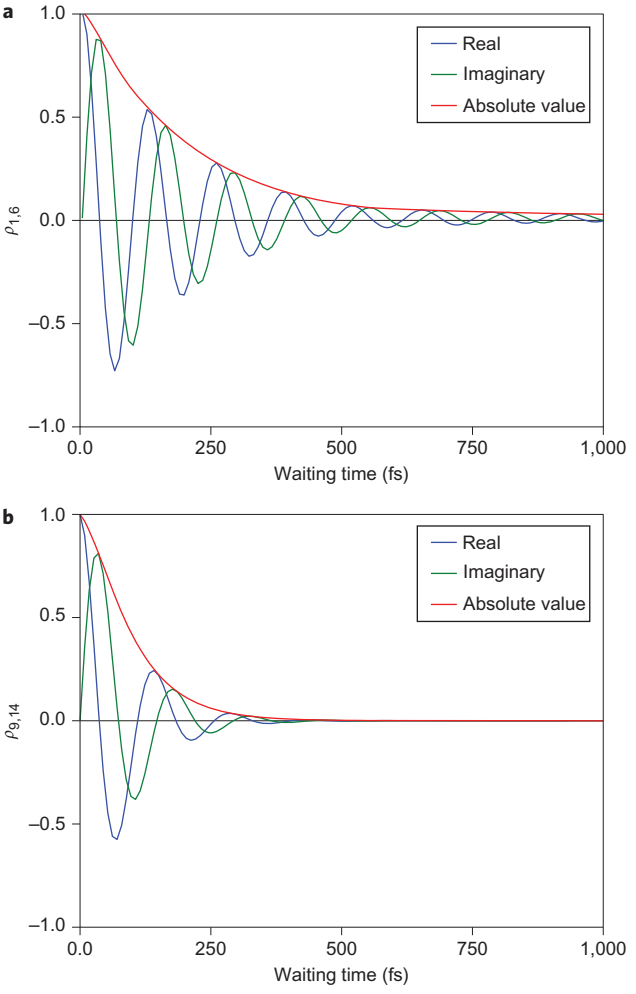

Figure 3 | Simulations of decay curves for coherence elements of the density matrix between pairs of excitons within monomeric LHCII. The two decay timescales indicate two different regimes of behaviour. **a**, Excitons 1 and 6 are primarily localized on two strongly coupled Chl (611–612)[36], and thus exhibit long-lived coherence. **b**, Excitons 9 and 14 are localized on two weakly coupled Chl (601 and 605, respectively)[36], and thus exhibit short-lived coherence.

therefore adopted the spectral density used in the numerical fitting of 2D electronic spectra of the Fenna–Matthews–Olson complex isolated from green sulfur bacteria[31]. Figure 3a shows the time evolution of the coherence between excitons $|e_1\rangle$ and $|e_6\rangle$, given as

$$\begin{aligned} |e_1\rangle &\simeq 0.18|a602\rangle + 0.57|a610\rangle + 0.45|a611\rangle - 0.65|a612\rangle \\ |e_6\rangle &\simeq 0.84|a611\rangle + 0.53|a612\rangle \end{aligned} \quad (6)$$

where $|n\rangle$ ($n = 601 - 614$) represents the state where only the nth chlorophyll site is in its excited electronic state and all others are in their ground electronic states. We have ignored the superposition coefficients with absolute values smaller than 0.1. In this case, the two excitons that share the most strongly coupled pigments in LHCII are Chl-*a* 611 and Chl-*a* 612 (ref. 36), and the quantum coherence exhibits a lifetime of at least 1 ps. Figure 3b, on the other hand, shows a case where excitonic quantum coherence decays quickly. The coherence shown is between excitons $|e_9\rangle$ and $|e_{14}\rangle$,

$$\begin{aligned} |e_9\rangle &\simeq 0.99|b605\rangle \\ |e_{14}\rangle &\simeq 0.97|b601\rangle - 0.10|b606\rangle - 0.15|b607\rangle \end{aligned} \quad (7)$$

which do not share the same pigments; they are almost completely localized on Chl-*b* 605 and Chl-*b* 601, respectively.

Although two of the present authors investigated the physical origins of long-lived electronic quantum coherence, specifically addressing the finite timescales of protein-induced fluctuations/dissipations[7,37,38], here we consider a necessary condition for long-lived coherence in a simpler way and examine the relation between experimentally observed quantum beating in exciton space and the spatial dynamics of electronic excitation through a PPC. The energy gap between the ground state with zero excitations, $|0\rangle$, and the μth exciton in the single-excitation manifold, $|e_\mu\rangle$, can be separated into the ensemble-averaged value and fluctuation, $E_\mu(t) = E_\mu^{\mathrm{av}} + \delta E_\mu(t)$. The dephasing of the $0 - e_\mu$ coherence is described by the correlation function

$$C_{\mu\mu}(t) = \langle \delta E_\mu(t)\delta E_\mu(0)\rangle \tag{8}$$

On the other hand, the fluctuating energy gap between excitons $|e_\mu\rangle$ and $|e_\nu\rangle$ is given as

$$E_\mu(t) - E_\nu(t) = [E_\mu^{\mathrm{av}} - E_\nu^{\mathrm{av}}] + [\delta E_\mu(t) - \delta E_\nu(t)] \tag{9}$$

so the dephasing of the $e_\mu - e_\nu$ coherence is described by

$$\begin{aligned} S_{\mu\nu}(t) &= \langle [\delta E_\mu(t) - \delta E_\nu(t)][\delta E_\mu(0) - \delta E_\nu(0)]\rangle \\ &= C_{\mu\mu}(t) + C_{\nu\nu}(t) - C_{\mu\nu}(t) - C_{\nu\mu}(t) \end{aligned} \tag{10}$$

where $C_{\mu\nu}(t)$ is the cross-correlation function $C_{\mu\nu}(t) = \langle \delta E_\mu(t)\delta E_\nu(0)\rangle$. If two excitons $|e_\mu\rangle$ and $|e_\nu\rangle$ share the same pigments or are spatially overlapped, the fluctuations $\delta E_\mu(t)$ and $\delta E_\nu(t)$ contain the same components and hence the cross-correlation function does not vanish. In this situation, the root-mean-squared amplitude of the fluctuations is $[S_{\mu\nu}(0)]^{1/2} = [C_{\mu\mu}(0) + C_{\nu\nu}(0) - C_{\mu\nu}(0) - C_{\nu\mu}(0)]^{1/2}$. The amplitude of the fluctuation is reduced by the presence of cross-correlation resulting from spatial overlap of the excitons, and therefore the quantum superposition between them is more resistant to destruction. To clarify this point, we consider a coupled dimer with a Hamiltonian given as

$$\begin{aligned} H = {} & \hbar\left[\Omega_1 + \delta\Omega_1(t)\right]|1\rangle\langle 1| + \hbar\left[\Omega_2 + \delta\Omega_2(t)\right]|2\rangle\langle 2| \\ & + \hbar J_{12}\left[|1\rangle\langle 2| + |2\rangle\langle 1|\right] \end{aligned} \tag{11}$$

where $\hbar\Omega_m$ and $\hbar\delta\Omega_m(t)$ are the Franck–Condon energy and fluctuations in the electronic transition energy of pigment m, respectively. $\hbar J_{12}$ represents the electronic coupling between pigments 1 and 2. We assume $\langle \delta\Omega_1(t)\delta\Omega_2(0)\rangle = 0$ to focus on the importance of spatial overlap between excitons. This cross-correlation function is discussed in detail in refs 13, 39. $S_{12}(t)$ in this dimer system can be expressed as

$$S_{12}(t) = \hbar^2(\cos 2\phi)^2 \sum_{m=1,2} \langle \delta\Omega_m(t)\delta\Omega_m(0)\rangle \tag{12}$$

where ϕ is the mixing angle $2\phi = \arctan[2J_{12}/(\Omega_1 - \Omega_2)]$ and $0 \le |2\phi| < \pi/2$. Therefore, the root-mean-squared amplitude of the fluctuating energy gap between excitons $|e_1\rangle$ and $|e_2\rangle$ decreases as the mixing angle increases. Thus, the larger the absolute value of the electronic coupling J_{12} for a fixed energy gap Ω_1–Ω_2 is, the longer the lifetime of the excitonic quantum superposition. When electronic excitations are localized on sites ($\phi \cong 0$), $S_{12}(t)$ reduces to a sum of the correlation functions of site energy fluctuations. In this situation, the dephasing of the e_1–e_2 coherence is essentially the same as that of the electronic transitions of the individual pigments. This is a complementary view to the adiabatic excitonic energy surface used for understanding the physical mechanism of long-lived coherence in the case of strong reorganization energy[37]. Using a picture of an adiabatic energy surface, the energy barrier separating two pigments decreases as the electronic coupling increases in magnitude, and thus the lifetime of the quantum coherence is enhanced. For these reasons, quantum coherence between $|e_1\rangle$ and $|e_6\rangle$ in equation (6) exhibits a longer lifetime, whereas that between $|e_9\rangle$ and $|e_{14}\rangle$ in equation (7) does not. In addition, because the excitons responsible for these beating peaks originate from electronic excitations on pigments, coherent dynamics can be mapped back onto the site representation. Wave-like motion in the site representation occurs only when excitons share the same pigments with a large mixing angle. For example, a superposition between the excitons in equation (6) corresponds to a wave packet between Chl-*a* 611 and Chl-*a* 612. A time-evolving superposition, $e^{-iE_1t}|e_1\rangle + e^{-iE_6t}|e_6\rangle$, yields time-dependent probabilities of finding the states $|a611\rangle$ and $|a612\rangle$ of $P_{a611}(t) \propto 0.91 + 0.76\cos[(E_6 - E_1)t/\hbar]$ and $P_{a612}(t) \propto 0.70 - 0.69\cos[(E_6 - E_1)t/\hbar]$, respectively. Even if excitons that do not share the same pigments, for example, the excitons in equation (7), show a long-lived superposition, this has absolutely no connection with wave-like energy transfer in the site representation. Short-lived superpositions of excitons created by broadband excitation, but which do not share the same pigments, have no connection to the wave-like energy transfer indicated by the long-lived superpositions observed after the decay of the 'trivial' superpositions. A time-evolving superposition, $e^{-iE_9t}|e_9\rangle + e^{-iE_{14}t}|e_{14}\rangle$, leads to time-independent probabilities of observing states $|b601\rangle$, $|b605\rangle$, $|b606\rangle$ and $|b607\rangle$. Namely, superpositions between excitons that do not share the same pigments (small mixing angles) give Förster-type incoherent energy transfer.

Discussion

In monomeric LHCII, after the first two light–matter interactions of the four-wave mixing experiment, there are 182 (14×13) potential combinations of excitonic states that produce coherences during the waiting time, or $\rho(t=0) = |e_i\rangle\langle e_j|$, $i \neq j$, where ρ is the density operator and $|e_i\rangle$ is an exciton. There are, however, only 14 possible populations, $\rho(t=0) = |e_i\rangle\langle e_i|$. Because of the order of magnitude difference in the number of combinations, these coherences combine to contribute a large amount of amplitude to the 2D spectra. However, these coherences decay rapidly. If the complete LHCII trimer is considered (containing 42 chlorophylls), there are 1,722 possible combinations that produce coherences. Thus, this may produce an increase in the relative amplitude of coherence to population contributions at short times with an increase in system size. We suggest that the short-time decay of the coherence signal arises from very rapid dephasing between the many pigments with vanishingly small couplings. The decay timescale from these short-lived coherences was determined using the all-parallel spectra, because this effect, although due to excitonic coherence, dominates the signal regardless of pulse polarization, due to the size of the system.

Although the theoretical results support an attribution of the rapid decay to weakly coupled coherences, there is no way to definitively rule out other factors. For example, the short-time decay may partially arise from pulse overlap effects[40], as the decay time is similar to the pulse duration. Finally, the loss of memory in the environment[37] on the environmental correlation timescale, which according to some models can be as short as 50 fs, causes a decrease in amplitude of the photon-echo component of the 2D signal[41]. An additional factor to note is that the measured timescales correspond to the timescales of these coherences in an ensemble, and so are limited by ensemble dephasing. Recent theoretical work indicates that the timescales of coherent motion in an individual PPC, which is of interest because light harvesting occurs in an individual PPC, may outlast those in the bulk, which suggests that our measured coherence decay is dominated by ensemble dephasing[42].

Thus, these experimentally determined timescales can be viewed as a lower bound, and as a source of insight into the role of coherence, rather than a definitive timescale for coherence in light harvesting.

Finally, an interesting potential extension of this technique could be that (assuming perfectly set laser polarizations), under this sequence, off-diagonal features in non-rephasing spectra show environment-induced coherence transfer. Environment-induced coherence transfer occurs when phase coherence between two excited states then evolves into phase coherence between one of the original states and a third exciton[38,43,44], so phase coherence is maintained through energy transfer. Although we do not have the polarization precision to completely suppress other, stronger off-diagonal features, some off-diagonal amplitude could be a signature of environment-induced coherence transfer. The right shoulder of the low energy Chl-*a* diagonal peak broadens within 100 fs and then decays by 500 fs, in agreement with dynamical and energetic expectations for environment-induced coherence transfer. Environment-induced coherence transfer is more likely when the energy gap remains similar through the transfer process and occurs within 100–200 fs (ref. 37). While experiments using other polarization and pulse sequences have accessed the signal from vibrational environment-induced coherence transfer[45,46], improving the precision of the pulse polarization so this technique could provide a more definitive measure of environment-induced coherence transfer would provide a new means to access this elusive process in the electronic regime.

Conclusions

Application of the technique described here to systems with resolved excitonic levels will allow for the elucidation of individual excitonic superpositions. These measurements will open a window into the heterogeneity of environmental reorganization energy and relaxation time and suggest whether such pigment–protein interactions are tuned to improve functionality[47]. Then, with future experimental and theoretical development, the use of the coherence-specific polarization offers the potential to explore a wider variety of coherence–related phenomena. Isolating and examining environment-induced coherence transfer, for example, offers a unique window into the dynamics of the surrounding environment. Generally, as observed here, the environment induces dephasing or destroys coherences between the excited states. In the case of environment-induced coherence transfer, 'transfer', in essence, means both annihilation of an old state and creation of a new state. In this case, the environment exhibits the surprising effect of creating coherence. Thus, the use of the coherence-specific polarization sequence not only investigates excited-state dynamics, but also provides a new means to access the dynamics in the surrounding environment.

Methods

Trimeric LHCII was isolated from *Arabidopsis thaliana* as described previously[48]. LHCII was dissolved in 50 mM HEPES buffer (pH 7.6) with *n*-dodecyl α-D-maltoside 0.03%, mixed with glycerol at 30:70 (v/v), placed in a 200 μm quartz cell and cooled to 77 K. An optical density of 0.13 for the sample was measured at 673 nm (per 200 μm).

The details of the experimental apparatus, data acquisition and analysis have been described in detail elsewhere[49,50]. In brief, a home-built Ti:sapphire oscillator seeded a home-built Ti:sapphire regenerative amplifier, which pumped a home-built non-collinear optical parametric amplifier to produce a 3.4 kHz pulse train of 80 nm bandwidth pulses centred at 650 nm and compressed to a duration of 22 fs (refs 28,51). During the experiment, the four beams (three beams with 6 nJ per pulse and a local oscillator attenuated by four orders of magnitude) were focused to a spot size of 100 μm.

The 2D apparatus was a diffractive optic-based design in which four beams in a box geometry were generated by a beamsplitter, followed by a transmissive grating optimized for the ±1 orders[49,52]. Each spectrum was constructed by scanning the delay between pulses 1 and 2 (the coherence time, τ). The waiting time (T), or the period over which the monitored dynamics occurred, was the delay between pulses 2 and 3 and was set by a retroflector delay stage. The signal emitted in the phase-matched direction, $\mathbf{k}_S = -\mathbf{k}_1 + \mathbf{k}_2 + \mathbf{k}_3$, collinear with the local oscillator, was heterodyne-detected using a spectrometer and charge coupled device camera to form the emission axis (ω_t). Achromatic, half-wave retarders inserted into beams 1, 2 and 3 controlled the linear polarization[23]. The coherence time was scanned from −566.5 fs to 566.5 fs for the all-parallel data (0°, 0°, 0°, 0°), and from −319 fs to 319 fs for the coherence-peak specific data (45°, −45°, 90°, 0°), where negative time points denote the arrival of pulse 2 before pulse 1 (ref. 32). For each waiting time, a Fourier transform over the coherence time axis produces the excitation axis (ω_τ).

Received 6 December 2011; accepted 14 February 2012; published online 25 March 2012

References

1. Blankenship, R. E. *Molecular Mechanisms of Photosynthesis* (Blackwell Science, 2002).
2. Dekker, J. P. & Boekema, E. J. Supramolecular organization of thylakoid membrane proteins in green plants. *Biochim. Biophys. Acta Bioenerg.* **1706,** 12–39 (2005).
3. Andrews, D. L., Curutchet, C. & Scholes, G. D. Resonance energy transfer: beyond the limits. *Laser Photon. Rev.* **5,** 114–123 (2011).
4. Collini, E. *et al.* Coherently wired light-harvesting in photosynthetic marine algae at ambient temperature. *Nature* **463,** 644–647 (2010).
5. Panitchayangkoon, G. *et al.* Long-lived quantum coherence in photosynthetic complexes at physiological temperature. *Proc. Natl Acad. Sci. USA* **107,** 12766–12770 (2010).
6. Engel, G. S. *et al.* Evidence for wavelike energy transfer through quantum coherence in photosynthetic systems. *Nature* **446,** 782–786 (2007).
7. Ishizaki, A. & Fleming, G. R. Theoretical examination of quantum coherence in a photosynthetic system at physiological temperature. *Proc. Natl Acad. Sci. USA* **106,** 17255–17260 (2009).
8. Mohseni, M., Rebentrost, P., Lloyd, S. & Aspuru-Guzik, A. Environment-assisted quantum walks in photosynthetic energy transfer. *J. Chem. Phys.* **129,** 174106 (2008).
9. Plenio, M. B. & Huelga, S. F. Dephasing-assisted transport: quantum networks and biomolecules. *New J. Phys.* **10,** 113019 (2008).
10. Scholes, G. D., Fleming, G. R., Olaya-Castro, A. & van Grondelle, R. Lessons from nature about solar light harvesting. *Nature Chem.* **3,** 763–774 (2011).
11. Fleming, G. R., Schlau-Cohen, G. S., Amarnath, K. & Zaks, J. Design principles of photosynthetic light-harvesting. *Faraday Discuss.* **155,** 27–41 (2012).
12. Cheng, Y. C. & Fleming, G. R. Coherence quantum beats in two-dimensional electronic spectroscopy. *J. Phys. Chem. A* **112,** 4254–4260 (2008).
13. Lee, H., Cheng, Y. C. & Fleming, G. R. Coherence dynamics in photosynthesis: protein protection of excitonic coherence. *Science* **316,** 1462–1465 (2007).
14. Mercer, I. P. *et al.* Instantaneous mapping of coherently coupled electronic transitions and energy transfers in a photosynthetic complex using angle-resolved coherent optical wave-mixing. *Phys. Rev. Lett.* **102,** 57402 (2009).
15. Calhoun, T. R. *et al.* Quantum coherence enabled determination of the energy landscape in light-harvesting complex II. *J. Phys. Chem. B* **113,** 16291–16295 (2009).
16. Zanni, M. T., Ge, N. H., Kim, Y. S. & Hochstrasser, R. M. Two-dimensional IR spectroscopy can be designed to eliminate the diagonal peaks and expose only the crosspeaks needed for structure determination. *Proc. Natl Acad. Sci. USA* **98,** 11265–11270 (2001).
17. Hochstrasser, R. M. Two-dimensional IR-spectroscopy: polarization anisotropy effects. *Chem. Phys.* **266,** 273–284 (2001).
18. Dreyer, J., Moran, A. M. & Mukamel, S. Tensor components in three pulse vibrational echoes of a rigid dipeptide. *Bull. Korean Chem. Soc.* **24,** 1091–1096 (2003).
19. Jonas, D. M. Two-dimensional femtosecond spectroscopy. *Annu. Rev. Phys. Chem.* **54,** 425–463 (2003).
20. Ginsberg, N. S., Cheng, Y. C. & Fleming, G. R. Two-dimensional electronic spectroscopy of molecular aggregates. *Acc. Chem. Res.* **42,** 1352–1363 (2009).
21. Schlau-Cohen, G. S., Ishizaki, A. & Fleming, G. R. Two-dimensional electronic spectroscopy and photosynthesis: fundamentals and applications to photosynthetic light-harvesting. *Chem. Phys.* **386,** 1–22 (2011).
22. Schlau-Cohen, G. S., Dawlaty, J. M. & Fleming, G. R. Ultrafast multidimensional spectroscopy: principles and applications to photosynthetic systems. *IEEE J. Sel. Top. Quantum Electron.* **18,** 283–295 (2012).
23. Read, E. L. *et al.* Cross-peak-specific two-dimensional electronic spectroscopy. *Proc. Natl Acad. Sci. USA* **104,** 14203–14208 (2007).
24. Schlau-Cohen, G. S. *et al.* Spectroscopic elucidation of uncoupled transition energies in the major photosynthetic light-harvesting complex, LHCII. *Proc. Natl Acad. Sci. USA* **107,** 13276–13281 (2010).
25. Ginsberg, N. S. *et al.* Solving structure in the CP29 light harvesting complex with polarization-phased 2D electronic spectroscopy. *Proc. Natl Acad. Sci. USA* **108,** 3848–3853 (2011).
26. Mukamel, S. *Principles of Nonlinear Optical Spectroscopy* (Oxford Univ. Press, 1995).
27. van Grondelle, R. & Novoderezhkin, V. I. Energy transfer in photosynthesis: experimental insights and quantitative models. *Phys. Chem. Chem. Phys.* **8,** 793–807 (2006).

28. Schlau-Cohen, G. S. *et al.* Pathways of energy flow in LHCII from two-dimensional electronic spectroscopy. *J. Phys. Chem. B* **113,** 15352–15363 (2009).
29. Liu, Z. F. *et al.* Crystal structure of spinach major light-harvesting complex at 2.72 ångstrom resolution. *Nature* **428,** 287–292 (2004).
30. Standfuss, R., van Scheltinga, A. C. T., Lamborghini, M. & Kuhlbrandt, W. Mechanisms of photoprotection and nonphotochemical quenching in pea light-harvesting complex at 2.5 Å resolution. *EMBO J.* **24,** 919–928 (2005).
31. Read, E. L. *et al.* Visualization of excitonic structure in the Fenna–Matthews–Olson photosynthetic complex by polarization-dependent two-dimensional electronic spectroscopy. *Biophys. J.* **95,** 847–856 (2008).
32. Ernst, R. R., Bodenhausen, G. & Wokaun, A. *Principles of Nuclear Magentic Resonance in One and Two Dimensions* (ed. Rowlinson, J. S.) (Oxford Science Publications, 1987).
33. Barzda, V. *et al.* Singlet–singlet annihilation kinetics in aggregates and trimers of LHCII. *Biophys. J.* **80,** 2409–2421 (2001).
34. Bittner, T., Irrgang, K. D., Renger, G. & Wasielewski, M. R. Ultrafast excitation-energy transfer and exciton–exciton annihilation processes in isolated light-harvesting complexes of Photosystem-II (LHC-II) from spinach. *J. Phys. Chem.* **98,** 11821–11826 (1994).
35. Ishizaki, A. & Fleming, G. R. Unified treatment of quantum coherent and incoherent hopping dynamics in electronic energy transfer: reduced hierarchy equation approach. *J. Chem. Phys.* **130,** 234111 (2009).
36. Frahmcke, J. S. & Walla, P. J. Coulombic couplings between pigments in the major light-harvesting complex LHC II calculated by the transition density cube method. *Chem. Phys. Lett.* **430,** 397–403 (2006).
37. Ishizaki, A., Calhoun, T. R., Schlau-Cohen, G. S. & Fleming, G. R. Quantum coherence and its interplay with protein environments in photosynthetic electronic energy transfer. *Phys. Chem. Chem. Phys.* **12,** 7319–7337 (2010).
38. Ishizaki, A. & Fleming, G. R. On the adequacy of the Redfield equation and related approaches to the study of quantum dynamics in electronic energy transfer. *J. Chem. Phys.* **130,** 234110 (2009).
39. Ishizaki, A. & Fleming, G. R. Quantum superpositions in photosynthetic light harvesting: delocalization and entanglement. *New J. Phys.* **12,** 055004 (2010).
40. Engh, R. A., Petrich, J. W. & Fleming, G. R. Removal of coherent coupling artifact in ground-state recovery experiments—malachite green in water–methanol mixtures. *J. Phys. Chem.* **89,** 618–621 (1985).
41. Joo, T. H., Jia, Y. W., Yu, J. Y., Lang, M. J. & Fleming, G. R. Third-order nonlinear time domain probes of solvation dynamics. *J. Chem. Phys.* **104,** 6089–6108 (1996).
42. Ishizaki, A. & Fleming, G. R. On the interpretation of quantum coherent beats observed in two-dimensional electronic spectra of photosynthetic light harvesting complexes. *J. Phys. Chem. B* **115,** 6227–6233 (2011).
43. Ohtsuki, Y. & Fujimura, Y. Bath-induced vibronic coherence transfer effects on femtosecond time-resolved resonant light-scattering spectra from molecules. *J. Chem. Phys.* **91,** 3903–3915 (1989).
44. Jean, J. M. & Fleming, G. R. Competition between energy and phase relaxation in electronic curve crossing processes. *J. Chem. Phys.* **103,** 2092–2101 (1995).
45. Khalil, M., Demirdoven, N. & Tokmakoff, A. Vibrational coherence transfer characterized with Fourier-transform 2D IR spectroscopy. *J. Chem. Phys.* **121,** 362–373 (2004).
46. Nee, M. J., Baiz, C. R., Anna, J. M., McCanne, R. & Kubarych, K. J. Multilevel vibrational coherence transfer and wavepacket dynamics probed with multidimensional IR spectroscopy. *J. Chem. Phys.* **129,** 084503 (2008).
47. Olbrich, C., Strumpfer, J., Schulten, K. & Kleinekathofer, U. Theory and simulation of the environmental effects on FMO electronic transitions. *J. Phys. Chem. Lett.* **2,** 1771–1776 (2011).
48. Caffarri, S., Croce, R., Breton, J. & Bassi, R. The major antenna complex of photosystem II has a xanthophyll binding site not involved in light harvesting. *J. Biol. Chem.* **276,** 35924–35933 (2001).
49. Brixner, T., Stiopkin, I. V. & Fleming, G. R. Tunable two-dimensional femtosecond spectroscopy. *Opt. Lett.* **29,** 884–886 (2004).
50. Brixner, T., Mancal, T., Stiopkin, I. V. & Fleming, G. R. Phase-stabilized two-dimensional electronic spectroscopy. *J. Chem. Phys.* **121,** 4221–4236 (2004).
51. Joo, T., Jia, Y. W. & Fleming, G. R. Ti-sapphire regenerative amplifier for ultrashort high-power multikilohertz pulses without an external stretcher. *Opt. Lett.* **20,** 389–391 (1995).
52. Cowan, M. L., Ogilvie, J. P. & Miller, R. J. D. Two-dimensional spectroscopy using diffractive optics based phased-locked photon echoes. *Chem. Phys. Lett.* **386,** 184–189 (2004).

Acknowledgements

This work was supported by the Director, Office of Science, Office of Basic Energy Sciences, of the US Department of Energy (contract DE-AC02-05CH11231) and the Division of Chemical Sciences, Geosciences, and Biosciences, Office of Basic Energy Sciences of the US Department of Energy (grant DE-AC03-76SF000098) (at LBNL and University of California, Berkeley). R.B. and M.B. acknowledge EU project PITN-GA-2009-238017 HARVEST and EU project 245070 FP7-KBBE-2009-3SUNBIOPATH. G.S.S.-C. thanks the A.A.U.W. American Fellowship and N.S.G. thanks the LBNL Glenn T. Seaborg postdoctoral fellowship for support.

Author contributions

G.S.S.-C. and G.R.F. conceived and designed the experiments. G.S.S.-C., T.R.C. and N.S.G. performed the experiments. G.S.S.-C. and A.I. analysed the data. A.I. performed theoretical calculations. M.B. and R.B. grew and purified the sample. G.S.S.-C. and A.I. co-wrote the paper. All authors discussed the results and commented on the manuscript.

Additional information

The authors declare no competing financial interests. Supplementary information accompanies this paper at www.nature.com/naturechemistry. Reprints and permission information is available online at http://www.nature.com/reprints. Correspondence and requests for materials should be addressed to G.R.F.